

Supporting Information

Scalable Thin-Layer Membrane Reactor for Heterogeneous and Homogenous Catalytic Gas-Liquid Reactions

Yiming Mo,[†] Joseph Imbrogno,[†] Haomiao Zhang and Klavs F. Jensen*

Department of Chemical Engineering, Massachusetts Institute of Technology
Cambridge, MA 02139, USA

Table of contents

1. General experiment and simulation details	2
2. Membrane reactor design and dimensions.....	2
3. Membrane reactor setup and detailed operation procedure	4
4. Estimation of the required purge stream flowrate for oxygenation reactions	5
5. 1-Dimensional model of membrane reactor	7
6. 3-Dimensional COMSOL simulation of membrane reactor	10
7. Comparison of heat transfer properties in packed-bed reactor and stacked membrane reactor.....	12
8. Stacked membrane reactor flow distribution simulation.....	13
9. Experimental reaction details	14
10. References	16

1. General experiment and simulation details

All reagents were purchased at the highest commercial quality and used without further purification. Yields were detected using gas chromatography (Agilent 6820) with dodecane calibrated as the internal standard. The samples for GC analysis were prepared by washing the reaction mixture with brine and then extracting the organic compounds using ethyl acetate.

All the individual components of membrane reactor were machined using Proto Labs' CNC service. Corresponding accessories (e.g. screws, nuts, O-ring, and insulation layer) were purchased from McMaster Carr.

Simulations were performed on Matlab (2018a) and COMSOL (5.3a).

2. Membrane reactor design and dimensions

The single-layer membrane reactor structure is illustrated in Fig. 1b. The detailed dimensions of individual components are as follows:

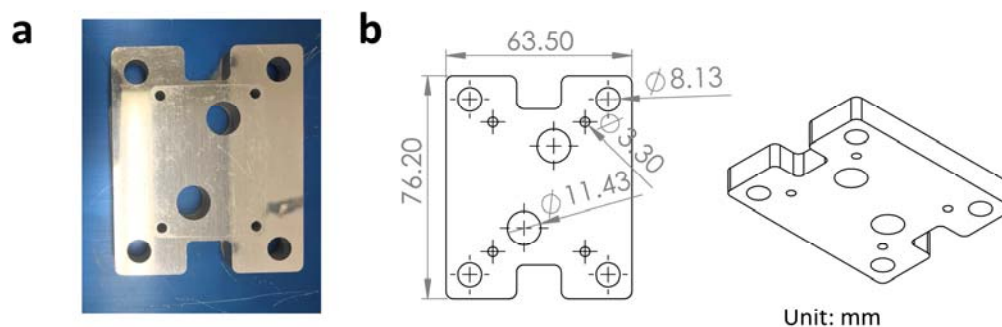


Fig. S1 (a) Photo of aluminum cover for single-layer membrane reactor. (b) Detailed dimensions of the aluminum cover for single-layer membrane reactor.

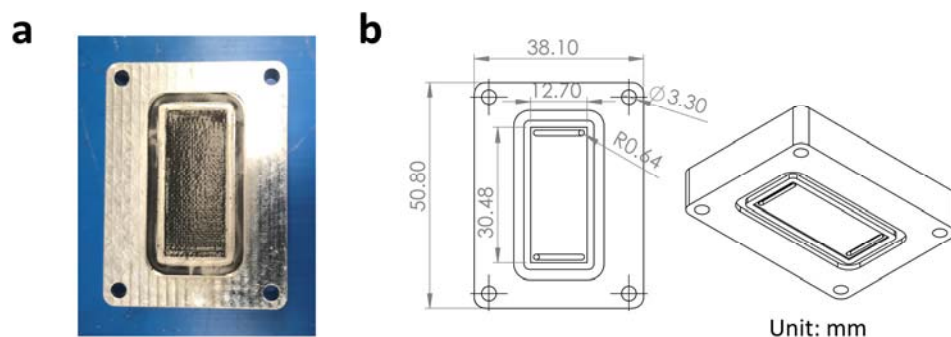


Fig. S2 (a) Photo of liquid distribution plate assembled with O-ring, Teflon AF membrane and carbon cloth for single-layer membrane reactor. (b) Detailed dimensions of the liquid distribution plate for single-layer membrane reactor.

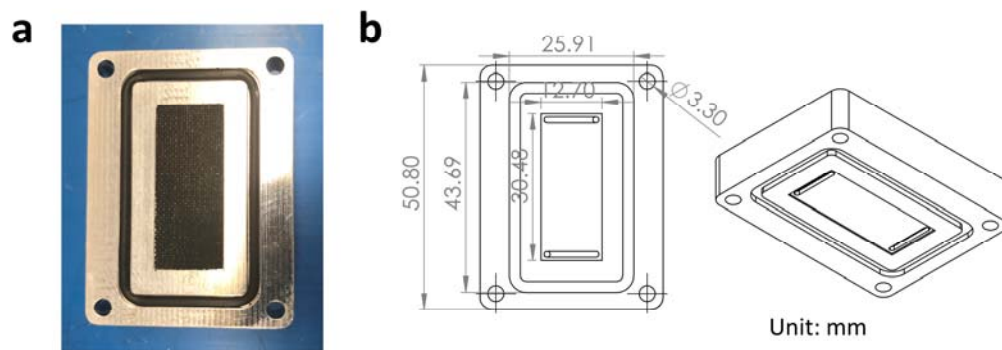


Fig. S3. (a) Photo of gas distribution plate assembled with O-ring and carbon cloth for single-layer membrane reactor. (b) Detailed dimensions of the gas distribution plate for single-layer membrane reactor.

The multi-layer membrane reactor structure is illustrated in Fig. 5b. The components of multi-layer membrane reactor structure are as follows:

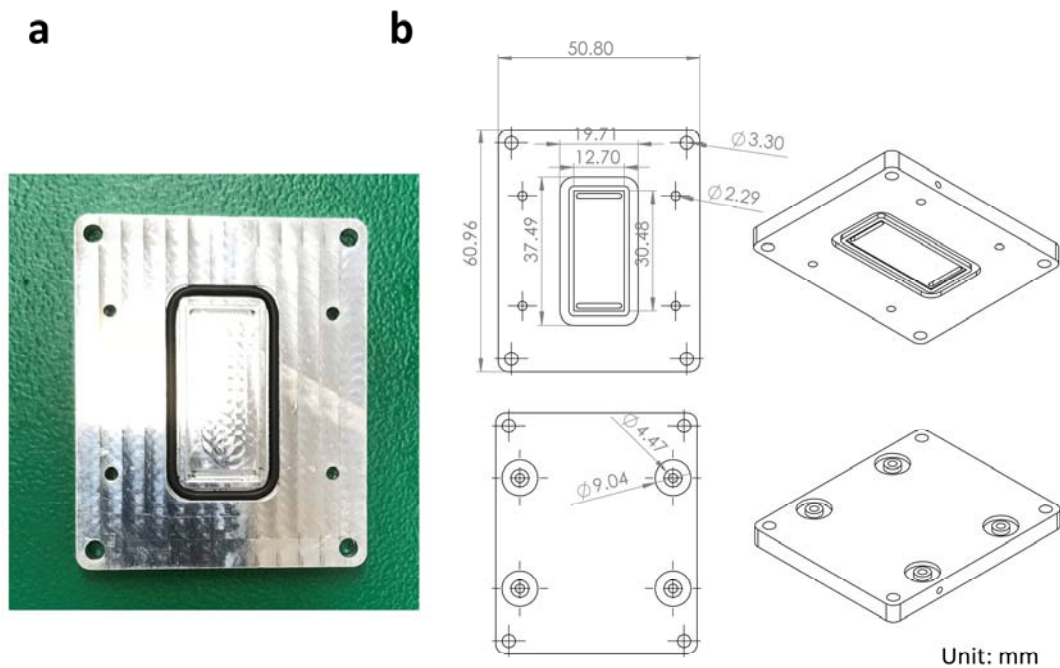


Fig. S4. (a) Photo of liquid distribution plate assembled with O-ring for multi-layer membrane reactor. (b) Detailed dimensions of the liquid distribution plate for multi-layer membrane reactor.

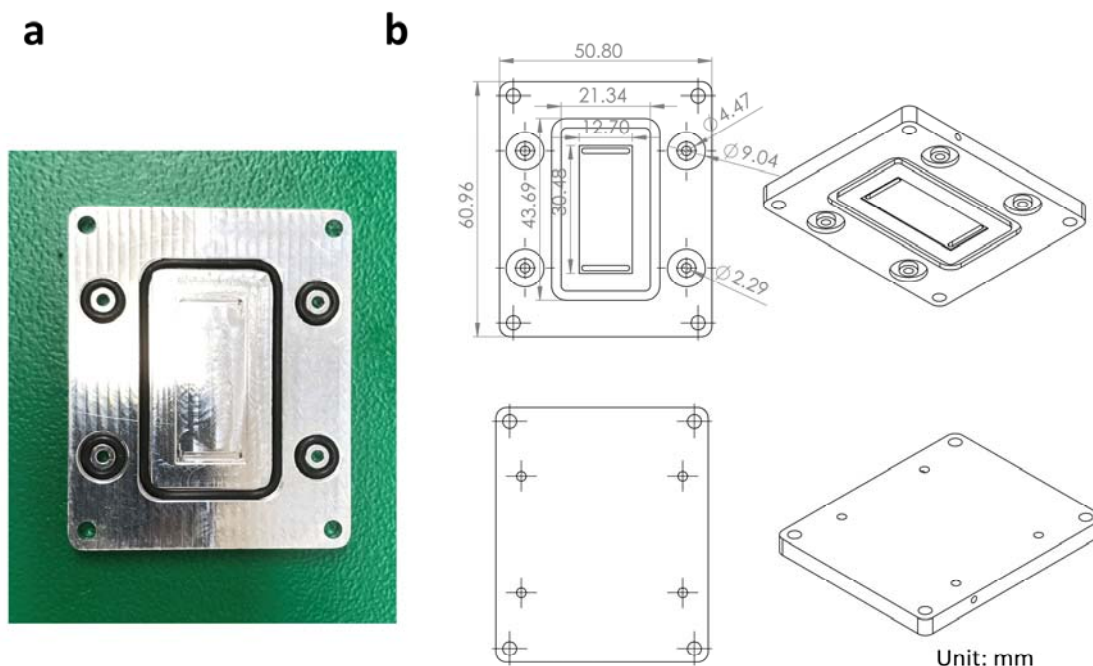


Fig. S5. (a) Photo of gas distribution plate assembled with O-ring for multi-layer membrane reactor. (b) Detailed dimensions of the gas distribution plate for multi-layer membrane reactor.

3. Membrane reactor setup and detailed operation procedure

General Assembly: The module was assembled as follows: the carbon cloth (with or without catalyst) was cut to a rectangle and then placed into the liquid flow channel. The Teflon AF membrane was cut to a larger rectangle and placed on top of the catalyst cloth in the liquid flow channel. A piece of catalyst-free carbon cloth was also placed in the flow channel on the gas side. The liquid and gas flow halves of the module were then assembled and sandwiched between two aluminum plates. O-rings were used to seal the flow channels and the two plates were screwed together in order to ensure a gas-tight seal on the entire module.

General Start-Up: Prior to each experiment, the system was cleaned with an appropriate liquid solvent for each reaction on the liquid side and nitrogen on the gas side. The liquid side was filled with the liquid reagent stream using an HPLC pump (Fig. S6a) and then the gas side was allowed to slowly pressurize, while maintaining a small (~150 kPa) difference between the back-pressure regulator (BPR) on the liquid side and the gas side. This was necessary to prevent gas from passing through the BPR and avoid rupturing the membrane. The reaction gas flow was controlled using a mass flow controller (Fig. S6b) and the variable BPR (Fig. S6c) was pressurized using nitrogen gas controlled by a pressure controller (Fig. S6c). Heating elements were turned on once the set point was reached and were controlled using a temperature controller with feedback from a thermocouple.

General Operation: Once the gas side pressure had reached the appropriate set-point, the liquid flow was started and the system was run for a time equal to three residence times of the system, based on flow rate, in order to reach steady state operation. Once steady state was reached, samples were collected and reaction parameters such as temperature and flow rates (constant flow rate ratio) were varied in order to determine the effect of temperature and residence time on the various reactions.

General Shut-down: The liquid and gas flow rates were stopped and then, simultaneously, the liquid and gas outlets were switched to their venting positions through a six-way valve (Fig. S6d), allowing for safe de-pressurization of the system and avoiding membrane rupture. The BPR pressure was also reduced to zero at this time. After every experiment, the system was flushed with the same solvent used during the experiment on the liquid side and nitrogen on the gas side.

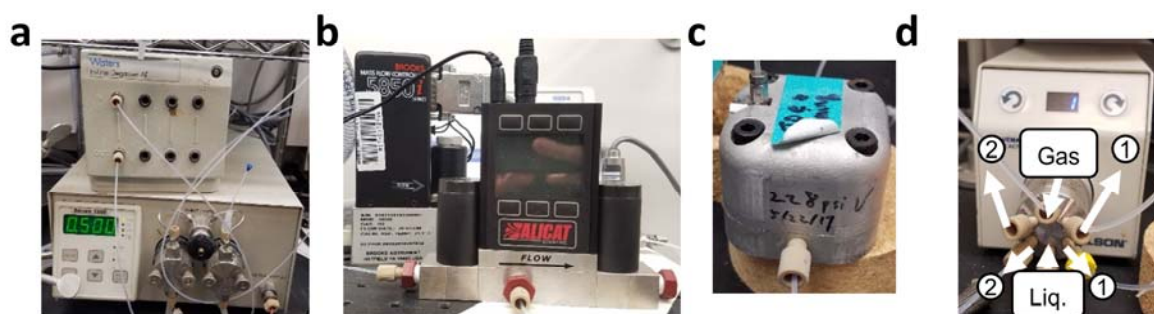


Fig. S6. Pictures of equipment used for controlling the gas-liquid membrane reactor: (a) gas flow controller for H₂ and O₂ (back) and pressure controller for N₂ used to pressurize the BPR (front), (b) in-line degasser (top) and HPLC pump (bottom), (c) variable BPR, and (d) 2 position 6-way valve for controlling the gas and liquid halves of the reactor. Position 1 is the venting position (used during startup and shutdown) and position 2 is used during operation of the reactor.

4. Estimation of the required purge stream flowrate for oxygenation reactions

For oxygenation reactions, even though the explosive mixture of liquid organic solvents and oxygen is avoided with the Teflon AF membrane, the organic solvent vapors could potentially penetrate through the membrane to the gas side, which raises safety concerns for large-scale applications. Unlike hydrogenation reactions in the membrane reactor, where the gas side outlet is plugged to reduce the unnecessary hydrogen consumption, additional oxygen purge stream could be required to avoid the accumulation of organic solvent vapors in the gas side to form explosive vapor.

In order to instruct safe membrane reactor operation for oxygenation reactions, a strategy was developed to calculate the required flowrate of oxygen purge stream to keep the solvent vapor concentration under the lower explosive limit (LEL). Since the LEL data of organic solvents in pure oxygen is rarely available, we took the approach developed by Chen¹ of estimating the LEL

in the pure oxygen using the LEL in the air. The equation to estimate the LEL of organic solvents in pure oxygen is shown as following:

$$LEL_{O_2} = \frac{LEL_{air}\hat{C}_{P_{O_2}}}{LEL_{air}\hat{C}_{P_{O_2}} + (1 - LEL_{air})(0.21\hat{C}_{P_{O_2}} + 0.79\hat{C}_{P_{N_2}})} \quad (1)$$

where LEL_{O_2} is lower explosive limit in pure oxygen, and LEL_{air} is the lower explosive limit in air. $\hat{C}_{P_{O_2}}$ is the average heat capacity of oxygen, and $\hat{C}_{P_{N_2}}$ is the average heat capacity of nitrogen.

The diffusion data of organic solvent molecules in the Teflon AF membrane is available from several previous publications.²⁻⁶ The data for several common organic solvents is shown in Table S1.

Table S1. Data used for estimating flowrate of oxygen purge stream

	LEL	LEL in O ₂	MW (g/mol)	Boiling point (°C)	Sorption parameter S ₀ @25 °C (g/100 g)	D ₀ @25 °C (m ² /s)	ΔH _s (kJ/mol)	E _D (kJ/mol)
Acetone	0.026	0.0245	58.08	56.0	2.43	7.67E-11	-35.8	18.8
Methanol	0.06	0.0566	32.04	64.7	1.84	1.60E-11	-44.6	33.9
Ethanol	0.033	0.0311	46.07	78.4	2.81	7.09E-12	-48.4	23.2
Cyclohexane	0.013	0.0122	84.16	80.75	6.75	1.61E-12	-35.2	15.8

The sorption parameter determines the concentration of organic solvent in the Teflon AF membrane, which has a temperature dependence as described in Eq. (2). The diffusion coefficient of organic molecule in the membrane also depends on the temperature (Eq. (3)).

$$S = S_0 \exp(-\Delta H_s / RT) \quad (2)$$

$$D = D_0 \exp(-E_D / RT) \quad (3)$$

The model used to estimate the purge stream is shown in Fig. S7. The diffusion of organic solvent vapor in the gas phase is orders of magnitudes larger than that in the membrane. Thus, we can assume the gas side is a homogenous mixture of organic solvent vapor and oxygen. Even though other substrates in the reaction mixture can also potentially penetrate through the membrane, those substrates were neglected considering their much lower volume concentration, slower diffusion rate, and higher boiling points compared to the organic solvent.

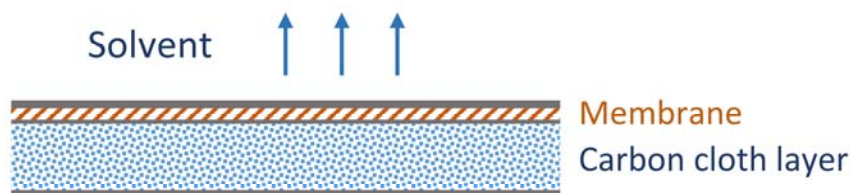


Fig. S7. Schematics of the membrane reactor for estimating the required purge stream.

We can estimate the flowrate of the purge stream with following equation:

$$Flowrate = DA_{mem.} \frac{C_{sat.}}{d_{mem.}} \left(1 - \frac{LEL_{O_2} * p}{p_{sat.}}\right) / C_{sol} \quad (4)$$

$$C_{sol} = r_{safety} * LEL_{O_2} * \frac{p}{RT} \quad (5)$$

$$\log(p_{sat.}) = A - \frac{B}{C + T} \quad (6)$$

where D is the diffusion coefficient of the organic solvent molecule in the Teflon AF membrane. $A_{mem.}$ is the surface area of the membrane, $C_{sat.}$ is the saturated organic solvent concentration in the gas phase, $d_{mem.}$ is the thickness of the membrane, p is the absolute pressure on the gas side, and $p_{sat.}$ is the saturated organic solvent partial pressure, which can be calculated by Antoine equation (Eq. (6)). C_{sol} is the upper limit of organic solvent concentration in the gas phase, which can be determined with Eq. (5). r_{safety} is the safety ratio (ranging from 0 to 1). Safety ratio of 0 corresponds to no tolerance to any solvent vapor in the gas phase, while the value of 1 corresponds to the largest tolerance operating at the lower explosive limit.

With this approach, the required flowrate of purge stream under different temperature for various organic solvents was determined, as shown in Fig. 2.

5. 1-Dimensional model of membrane reactor

COMSOL 3-D simulation shows a uniform liquid phase flow distribution across the carbon cloth, and a “plug-flow” velocity profile in the cross section of the carbon cloth (Fig. S8a). Compared to the scenario without porous carbon cloth (Fig. S8b), the porous structure simplifies the hydrodynamics making it possible to understand the system with a one-dimensional (1-D) model.

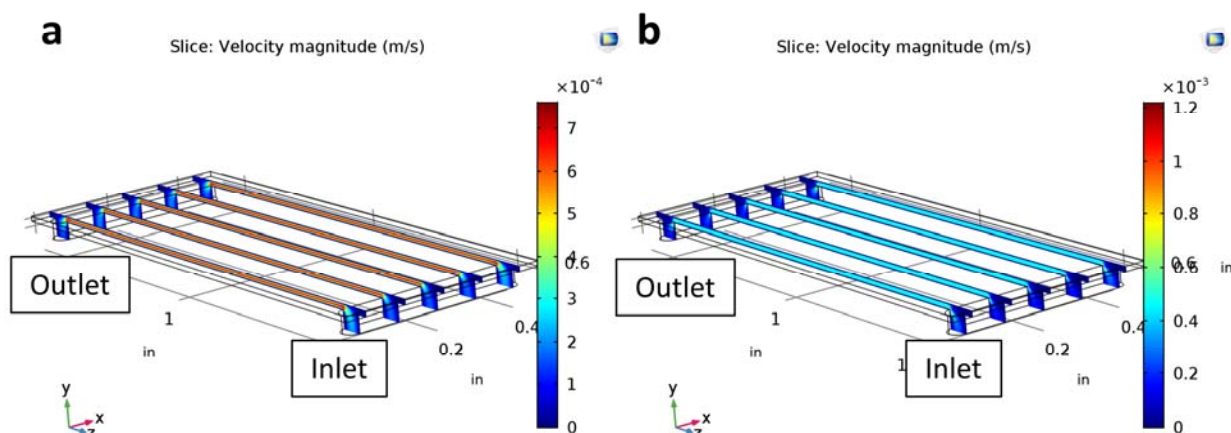


Fig. S8. Flow velocity profile in membrane reactor. (a) Membrane reactor without porous carbon cloth. (b) Membrane reactor with porous carbon cloth.

1-D model is illustrated in Fig. S9. Hydrogenation of nitrobenzene with ethanol as solvent is simulated in the 1-D model. Nitrobenzene (A) is fed into the membrane with a concentration of $C_{A,0}$, and a velocity of U . Hydrogen diffuses through the membrane to the catalytic region to react with nitrobenzene to form the hydrolysis product. With finite element analysis, the mass balance equations can be formulated as:

$$UC_A(x) = UC_A(x + \Delta x) + \Delta x k R(C_A, C_{H_2}) \quad (7)$$

$$UC_{H_2}(x) + \Delta x k_L a (C_{H_2,0} - C_{H_2}) = UC_{H_2}(x + \Delta x) + \Delta x k R(C_A, C_{H_2}) \quad (8)$$

where x indicates the location in the membrane reactor with range from 0 to L , (L is the length of the membrane reactor), k is the kinetic constant of the hydrogenation with the unit of s^{-1} , $R(C_A, C_{H_2})$ is the rate dependence on concentrations of nitrobenzene and hydrogen,⁷ and $k_L a$ is the mass transfer coefficient, which determines the rate of hydrogen diffusion into the catalytic regime. $k_L a$ is defined in the 1-D model, and it can be calculated with a 3-D simulation shown in a later section.

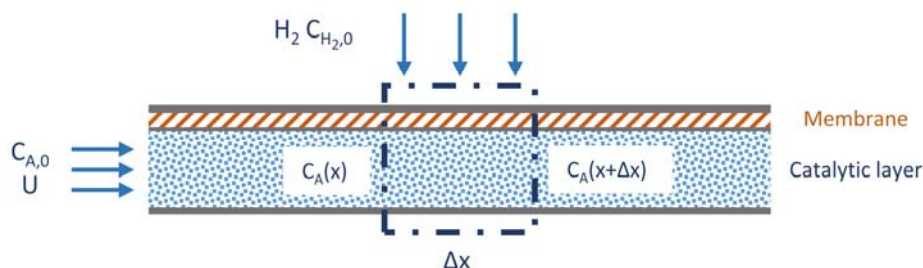


Fig. S9. The schematics of the 1-D model.

Simplifying Eq. (7) and (8), we can obtain the following equations:

$$-\frac{1}{Da_I} \frac{dC_A}{d\xi} = R(C_A, C_{H_2}) \quad (9)$$

$$-\frac{1}{Da_I} \frac{dC_{H_2}}{d\xi} = R(C_A, C_{H_2}) - \frac{1}{Da_{II}} (C_{H_2,0} - C_{H_2}) \quad (10)$$

$$\xi = \frac{x}{L} \quad (11)$$

$$Da_I = k \frac{L}{U} = k\tau \quad (12)$$

$$Da_{II} = \frac{k}{k_L a} \quad (13)$$

τ is the residence time in the membrane reactor calculated with Eq. (11). Da_I denotes the reaction time scale versus the residence time, which can roughly indicate the reaction conversion for homogeneous single-phase reaction. Da_{II} is introduced due to the diffusion of gas through membrane and liquid phase, which represents the ratio between reaction time scale and diffusion time scale.

As shown in Eq. (9) and (10), the system behavior is controlled by two dimensionless numbers (Da_I and Da_{II}). The dependence of the reaction conversion at the outlet of the membrane can be calculated by varying the values of two dimensionless numbers. (Fig. S10) When $Da_{II} \ll 1$, indicating the reaction rate is much slower than the diffusion rate, the reaction conversion in the membrane reactor is insensitive to the value of Da_{II} , corresponding to the “reaction limited” regime. In contrast, the dependence of the reaction conversion on Da_{II} becomes much stronger when $Da_{II} > 1$, corresponding to the “mass transfer limited” regime. Thus, identifying the ratio between the mass transfer time scale and reaction time scale is essential for choosing the optimal membrane reactor design (i.e. carbon cloth layer thickness) in order to balance the trade-off between productivity and reactor fabrication cost.

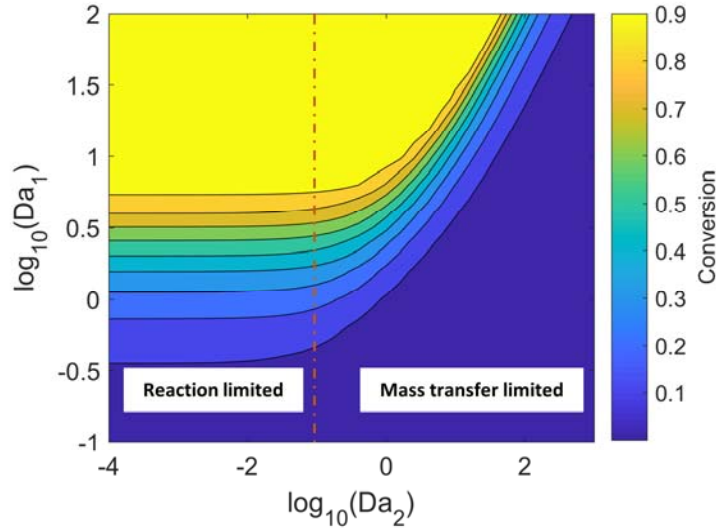


Fig. S10. The reaction conversion dependence on Da_I and Da_{II} .

The results of the 1-D simulation identified two critical dimensionless numbers (Da_I and Da_{II}), which can instruct the 3-D simulation in COMSOL.

6. 3-Dimensional COMSOL simulation of membrane reactor

The 3-D COMSOL simulation was conducted with and without reaction. In order to evaluate the mass transfer coefficient (k_{LA}) for various thickness of carbon cloth, mass transfer of hydrogen into ethanol was simulated in the membrane reactor. A typical hydrogen concentration profile in the membrane reactor is shown in Fig. S11, where hydrogen gradually saturates the liquid stream along the flow direction. Fig. 3 illustrates the dependence of k_{LA} on the carbon cloth thickness.

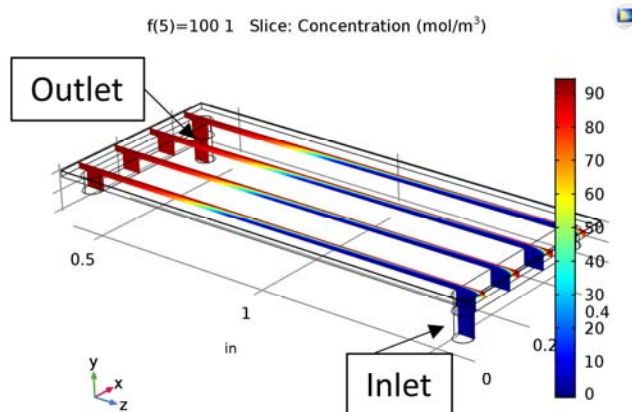


Fig. S11. The hydrogen concentration profile in membrane reactor.
Carbon cloth thickness: 0.3mm.

To demonstrate the validity of the 1-D model proposed in the previous section, varying the values of Da_I and Da_{II} in the 3-D model can give the reaction conversion under various conditions (i.e. residence time, carbon cloth thickness, and reaction rate). As shown in Fig. 4, the results from 3-D simulation give similar patterns as the 1-D model, thereby validating the 1-D model.

The conditions used in the COMSOL simulation are indicated in Table S2, and the corresponding domains and boundaries described in the Fig. S12. Refer to COMSOL user's guide for detailed information about the equation parameters.^{8,9}

Table S2. Domain controlling equations and boundaries conditions used in the COMSOL simulation.

Domain	Fluid Flow	Mass Transfer
A (Liquid)	$\frac{1}{\epsilon_p} \rho (\mathbf{u} \cdot \nabla) \mathbf{u} - \frac{1}{\epsilon_p} \nabla \cdot \left[-p\mathbf{I} + \mu \frac{1}{\epsilon_p} (\nabla \mathbf{u} + (\nabla \mathbf{u})^T) \right] - \left(\mu \kappa^{-1} + \beta_F \mathbf{u} + \frac{Q_{br}}{\epsilon_p^2} \right) \mathbf{u} + \mathbf{F}$ <p>Brinkman Equation (Fluid flow in porous media)</p>	$\nabla \cdot (-D_{e,j} \nabla c_i) + \mathbf{u} \cdot \nabla c_i = R_i + S_i$ <p>Mass transfer in porous media</p>
	$\rho \nabla \cdot (\mathbf{u}) = Q_{br}$ <p>Continuity equation in porous media</p>	
B (Membrane)	NA	$\nabla \cdot (-D_i \nabla c_i) = 0$ <p>Diffusive mass transfer in membrane</p>

Boundary	Fluid Flow	Mass Transfer
1 (Inlet)	$\mathbf{u} = \mathbf{U}_0$	$c_i = c_{0,i}$
2 (Outlet)	$p = p_0$	$\nabla c_i = 0$
3 (Wall)	$\mathbf{u} = 0$	$-D_i \nabla c_i + \mathbf{u} c_i = 0$
4 (Liquid – Membrane Interface)		$\frac{c_{H_2,membrane}}{c_{H_2,liquid}} = He$ <p>Henry's Law boundary condition</p>
5 (Gas – Membrane Interface)	N.A.	$c_{H_2} = c_{H_2,gas}$

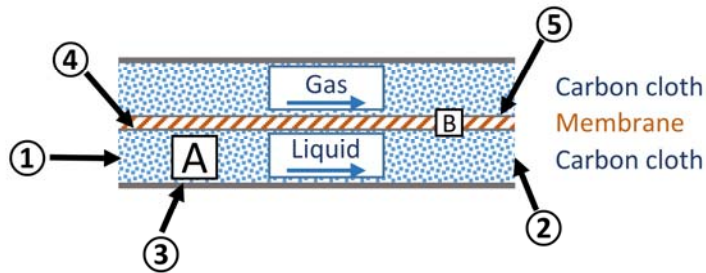


Fig. S12. The schematics of the membrane reactor showing the positions indicated in Table S2.

7. Comparison of heat transfer properties in packed-bed reactor and stacked membrane reactor

For highly exothermic reactions, a large-scale trickle-bed or packed-bed will suffer from insufficient heat transfer problems. The high temperature in the center of the reactor might lead to the decomposition of heat sensitive substrates. The membrane reactor designed in this work can efficiently solve the insufficient heat transfer problems for catalytic hydrogenation reactions. In order to preserve the heat transfer property of the single-layer reactor when stacking multiple layers together, cooling layers can be inserted between two layers as shown in Fig. S12.

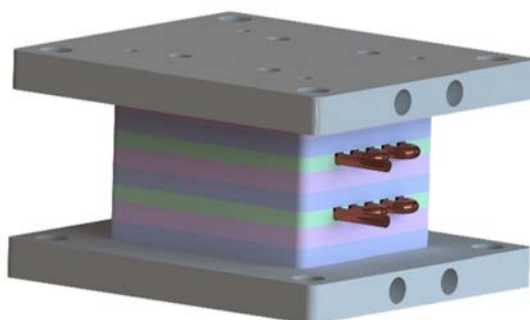


Fig. S13. The multi-layer membrane reactor with periodic cooling plates (green). Each cooling plate uses copper tubing for coolant. Gas distribution plates are shown in blue and liquid distribution plates are purple.

Since it is impractical to evaluate the heat transfer difference between a packed-bed reactor and a membrane reactor at the lab-scale, we employed COMSOL simulations to qualitatively compare the heat transfer rate between packed-bed reactor and membrane reactor in this work. We simulated an exothermic reaction in both reactors with the same reaction enthalpy and coolant capacity. As shown in Fig. S14, the packed-bed reactor has a comparatively long distance for heat dissipation, while membrane reactor has a very short heat dissipation distance when using periodic cooling plates. The centerline in the packed-bed reactor has the highest temperature, and the temperature difference between the reactor wall and centerline is much larger the temperature difference for the membrane reactor. Fig. S14b shows the maximum temperature in two reactors under different coolant flowrate. Increasing the coolant flowrate shows negligible reduction in maximum temperature since the heat dissipation of the packed-bed is insufficient to remove heat generated, while membrane reactor benefits significantly from the increased coolant flowrate due to better heat transfer capacity. The results demonstrate the advantages of the membrane reactor designed in this work for highly exothermic reactions at the large scale.

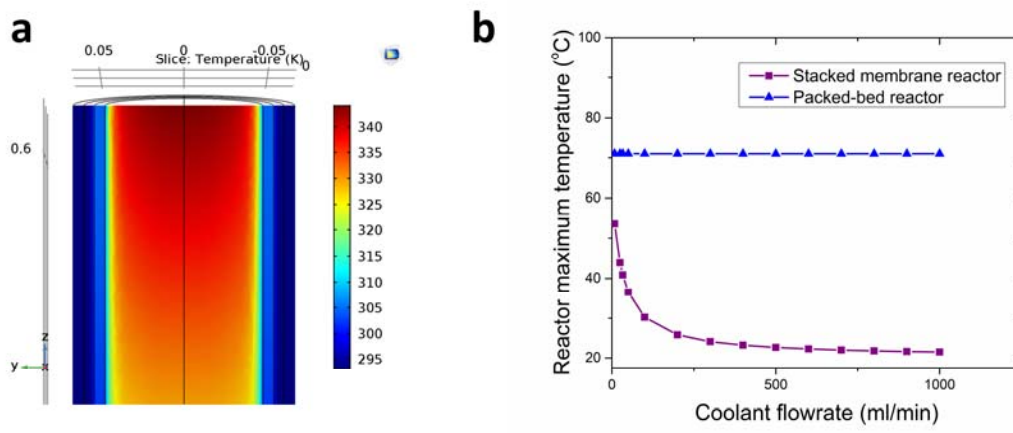


Fig. S14. (a) Temperature profile of a simulated packed-bed reactor. (b) The maximum temperature dependence on coolant flowrate in stacked membrane reactor and packed-bed reactor under the same reaction conditions.

8. Stacked membrane reactor flow distribution simulation

The flow distribution among the layers in the stacked membrane reactor significantly affects the scalability of the membrane reactor. Poor distribution will lead to different residence times in each layer, which might result in unconverted starting substrate. In addition, the results obtained from single-layer membrane reactor cannot be directly translated into multi-layer configuration, which causes the same issue of a tedious scale-up process as for a trickle-bed or packed-bed reactor. In order to enable direct scale-up from single-layer to multiple-layer, it is essential to have identical flow distribution across each layer in the stacked membrane reactor. Besides the optimized distribution channel design shown in Fig. 5a, the porous carbon cloth in each layer also plays an important role in unifying flow distribution. COMSOL hydrodynamics simulations illustrate the difference of flow distribution with and without carbon cloth for a 3-layer and 10-layer membrane reactor. (Fig. S15)

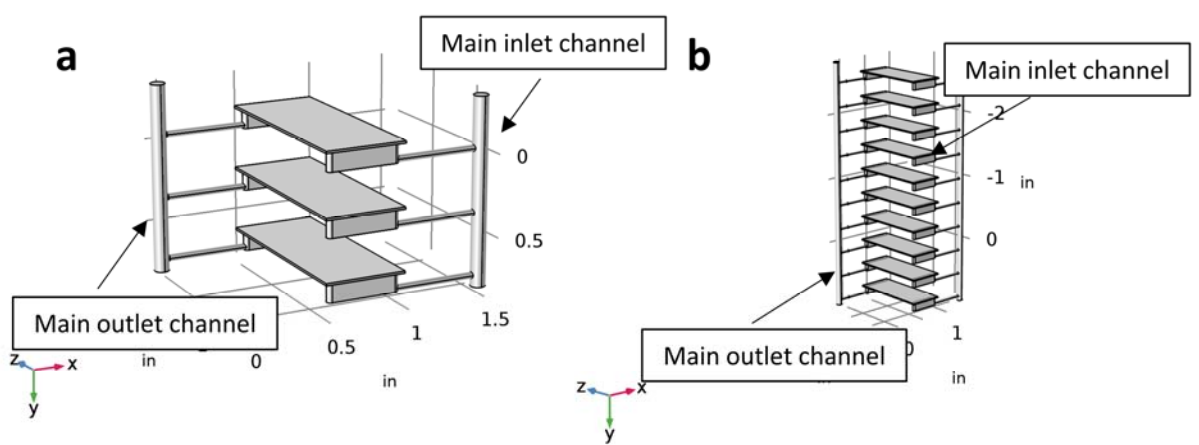


Fig. S15. The internal structure of stacked membrane reactor used for liquid hydrodynamics simulation in COMSOL. (a) The 3-layer stacked membrane reactor and (b) the 10-layer stacked membrane reactor.

The flowrate at the outlet of each layer is shown in Fig. S16. For the 3-layer stacked membrane reactor, the existence of the carbon cloth does not have a strong effect on the flow distribution; however, for the 10-layer stacked membrane reactor, the carbon cloth helps induce a uniform flow distribution.

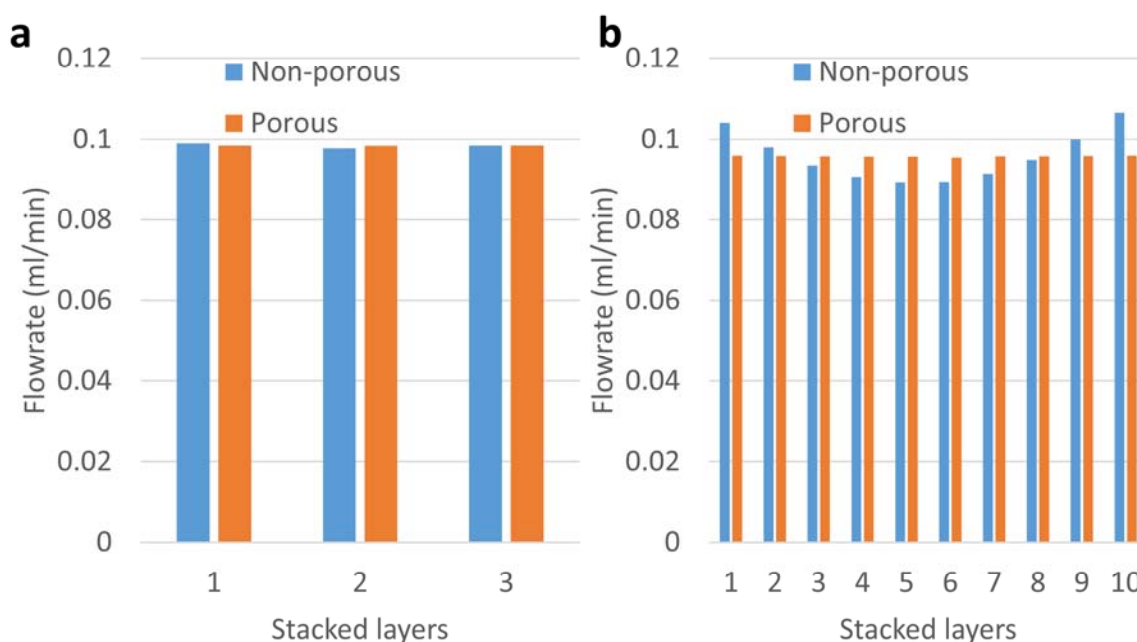
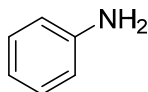
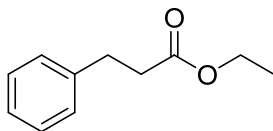


Fig. S16. The flowrate at the outlet of each layer for (a) 3-layer and (b) 10-layer stacked membrane reactor. Non-porous: the carbon cloth is absent from the liquid channel. Porous: carbon cloth is present in the liquid channel.

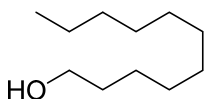
9. Experimental reaction details



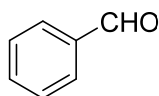
Aniline (1b). Prepared according to the general procedure using 0.8 mL of nitrobenzene (8.0 mmol, 1.0 equiv), carbon cloth with 4 mg/cm² Pd catalyst, and 39.2 mL of ethanol. Hydrogen gas was delivered to the system at 2.76 MPa (400 psig) and metered using a hydrogen mass flow controller. The liquid flow rate ranged from 0.05 to 0.10 mL/min (0.5 min – 1 min residence time) under a backpressure of 2.80 MPa (406 psig) and reaction temperature at 70 °C. The system was operated for a minimum of 3 residence times before collecting samples. The reaction mixture was subjected to analysis using GC-MS and compared with pure aniline purchased from Sigma Aldrich.



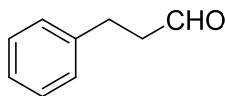
Ethyl 3-phenylpropanoate (2b). Prepared according to the general procedure using 3.0 mL of ethyl cinnamate (18.0 mmol, 1.0 equiv), carbon cloth with 4 mg/cm² Pd catalyst, and 27.0 mL ethyl acetate. Hydrogen gas was delivered to the system at 2.67 MPa (387 psig) and metered using a hydrogen mass flow controller. The liquid flow rate was set at 0.10 mL/min (0.5 min residence time) under a backpressure of 2.80 MPa (405 psig) and reaction temperature at 50 °C. The system was operated for a minimum of 3 residence times before collecting samples. The reaction mixture was subjected to analysis using GC-MS and compared with pure ethyl 3-phenylpropanoate purchased from Sigma Aldrich.



Undecan-1-ol (3b). Prepared according to the general procedure using 1.7 mL of 10-undecyn-1-ol (9.0 mmol, 1.0 equiv), carbon cloth with 4 mg/cm² Pd catalyst, and 28.3 mL ethyl acetate. Hydrogen gas was delivered to the system at 2.76 MPa (400 psig) and metered using a hydrogen mass flow controller. The liquid flow rate was set at 0.10 mL/min (0.5 min residence time) under a backpressure of 2.86 MPa (415 psig) and reaction temperature at 50 °C. The system was operated for a minimum of 3 residence times before collecting samples. The reaction mixture was subjected to analysis using GC-MS and compared with pure undecan-1-ol purchased from Sigma Aldrich.

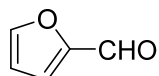


Benzaldehyde (4b). Prepared according to the general procedure using 0.6 mL benzyl alcohol (6.0 mmol, 1.0 equiv), 0.1 mg of tetrakisacetonitrile copper(I) triflate Cu(MeCN)₄(OTf) (0.3 mmol, 0.05 equiv), 0.05 g of 2,2'-bipyridine (0.3 mmol, 0.05 equiv), 0.05 mL of 1-methylimidazole (NMI) (0.6 mmol, 0.10 equiv), 0.05 g of (2,2,6,6-tetramethylpiperidin-1-yl)oxyl (TEMPO) (0.3 mmol, 0.05 equiv), and 30.0 mL acetonitrile. Acetonitrile was sparged with argon for 1 h to remove oxygen prior to experiment. The TEMPO and alcohol substrate were mixed together and added to 25.0 mL of acetonitrile. The remaining reagents were mixed and added to 5.0 mL acetonitrile. The solution was degassed before loading the solution into the system. Oxygen gas was delivered to the system at 0.74 MPa (108 psig) and metered using an oxygen mass flow controller. The liquid flow rate for the TEMPO/alcohol solution was 0.08 mL/min and the remaining solution was 0.02 mL/min (0.5 min residence time) under a backpressure of 0.79 MPa (115 psig) and reaction temperature at 30 °C. The system was operated for a minimum of 3 residence times before collecting samples. The reaction mixture was subjected to analysis using GC-MS and compared with pure benzaldehyde purchased from Sigma Aldrich.



3-phenyl-1-propanal (5b). Prepared according to the general procedure using 0.8 mL of 3-phenyl-1-propanol (6.0 mmol, 1.0 equiv), 0.1 mg of tetrakisacetonitrile copper(I) triflate Cu(MeCN)₄(OTf) (0.3 mmol, 0.05 equiv), 0.05 g of 2,2'-bipyridine (0.3 mmol, 0.05 equiv), 0.05 mL of 1-

methylimidazole (NMI) (0.6 mmol, 0.10 equiv), 0.05 g of (2,2,6,6-tetramethylpiperidin-1-yl)oxyl (TEMPO) (0.3 mmol, 0.05 equiv), and 30.0 mL acetonitrile. Acetonitrile was sparged with argon for 1 h to remove oxygen prior to experiment. The TEMPO and alcohol substrate were mixed together and added to 25.0 mL of acetonitrile. The remaining reagents were mixed and added to 5.0 mL acetonitrile. The solutions were degassed before loading the solution into the system. Oxygen gas was delivered to the system at 2.54 MPa (368 psig) and metered using an oxygen mass flow controller. The liquid flow rate for the TEMPO/alcohol solution was 0.04 mL/min and the remaining solution was 0.01 mL/min (1 min residence time) under a backpressure of 2.69 MPa (390 psig) and reaction temperature at 50 °C. The system was operated for a minimum of 3 residence times before collecting samples. The reaction mixture was subjected to analysis using GC-MS and compared with pure 3-phenyl-1-propanal purchased from Sigma Aldrich.



Furan-2-carbaldehyde (6b). Prepared according to the general procedure using 0.5 mL of furfuryl alcohol (6.0 mmol, 1.0 equiv), 0.1 mg of tetrakisacetonitrile copper(I) triflate $\text{Cu}(\text{MeCN})_4(\text{OTf})$ (0.3 mmol, 0.05 equiv), 0.05 g of 2,2'-bipyridine (0.3 mmol, 0.05 equiv), 0.05 mL of 1-methylimidazole (NMI) (0.6 mmol, 0.10 equiv), 0.05 g of (2,2,6,6-tetramethylpiperidin-1-yl)oxyl (TEMPO) (0.3 mmol, 0.05 equiv), and 30.0 mL acetonitrile. Acetonitrile was sparged with argon for 1 h to remove oxygen prior to experiment. The TEMPO and alcohol substrate were mixed together and added to 25.0 mL of acetonitrile. The remaining reagents were mixed and added to 5.0 mL acetonitrile. The solutions were degassed before loading the solution into the system. Oxygen gas was delivered to the system at 2.54 MPa (368 psig) and metered using an oxygen mass flow controller. The liquid flow rate for the TEMPO/alcohol solution was 0.08 mL/min and the remaining solution was 0.02 mL/min (0.5 min residence time) under a backpressure of 2.65 MPa (385 psig) and reaction temperature at 30 °C. The system was operated for a minimum of 3 residence times before collecting samples. The reaction mixture was subjected to analysis using GC-MS and compared with pure Furan-2-carbaldehyde purchased from Sigma Aldrich.

10. References

- 1 C.-C. Chen, *Ind. Eng. Chem. Res.*, 2011, **50**, 10283–10291.
- 2 V. I. Bondar, B. D. Freeman and Y. P. Yampolskii, *Macromolecules*, 1999, **32**, 6163–6171.
- 3 A. M. Polyakov, L. E. Starannikova and Y. P. Yampolskii, *J. Membr. Sci.*, 2003, **216**, 241–256.
- 4 A. M. Polyakov, L. E. Starannikova and Y. P. Yampolskii, *J. Membr. Sci.*, 2004, **238**, 21–32.
- 5 A. Polyakov, G. Bondarenko, A. Tokarev and Y. Yampolskii, *J. Membr. Sci.*, 2006, **277**, 108–119.
- 6 A. Tokarev, K. Friess, J. Machkova, M. Šipek and Y. Yampolskii, *J. Polym. Sci. Part B Polym. Phys.*, 2006, **44**, 832–844.
- 7 V. Holler, D. Wegricht, I. Yuranov, L. Kiwi-Minsker and A. Renken, *Chem. Eng. Amp Technol.*, 2000, **23**, 251–255.
- 8 CFD Module User's Guide, version 5.3a, www.comsol.com.
- 9 Chemical Reaction Engineering Module User's Guide, version 5.3a, www.comsol.com.